Reconstitution of ORP-mediated lipid exchange coupled to PI4P metabolism

Nicolas Fuggetta, Nicola Rigolli, Maud Magdeleine, Amazigh Hamaï, Agnese Seminara, Guillaume Drin

▶ **To cite this version:**

Nicolas Fuggetta, Nicola Rigolli, Maud Magdeleine, Amazigh Hamaï, Agnese Seminara, et al.. Reconstitution of ORP-mediated lipid exchange coupled to PI4P metabolism. Proceedings of the National Academy of Sciences of the United States of America, 2024, 121 (10), pp.e2315493121. 10.1073/pnas.2315493121 . hal-04766885

HAL Id: hal-04766885
https://hal.science/hal-04766885v1

Submitted on 5 Nov 2024

HAL is a multi-disciplinary open access archive for the deposit and dissemination of scientific research documents, whether they are published or not. The documents may come from teaching and research institutions in France or abroad, or from public or private research centers.

L'archive ouverte pluridisciplinaire **HAL**, est destinée au dépôt et à la diffusion de documents scientifiques de niveau recherche, publiés ou non, émanant des établissements d'enseignement et de recherche français ou étrangers, des laboratoires publics ou privés.

Distributed under a Creative Commons Attribution - NonCommercial - NoDerivatives 4.0 International License

PNAS RESEARCH ARTICLE | BIOPHYSICS AND COMPUTATIONAL BIOLOGY

Reconstitution of ORP-mediated lipid exchange coupled to PI4P metabolism

Nicolas Fuggetta[a,1], Nicola Rigolli[b,1], Maud Magdeleine[a,1], Amazigh Hamai[a], Agnese Seminara[c,2], and Guillaume Drin[a,2]

Edited by Pietro De Camilli, Yale University, New Haven, CT; received September 13, 2023; accepted January 24, 2024

Oxysterol-binding protein-related proteins (ORPs) play key roles in the distribution of lipids in eukaryotic cells by exchanging sterol or phosphatidylserine for PI4P between the endoplasmic reticulum (ER) and other cell regions. However, it is unclear how their exchange capacity is coupled to PI4P metabolism. To address this question quantitatively, we analyze the activity of a representative ORP, Osh4p, in an ER/Golgi interface reconstituted with ER- and Golgi-mimetic membranes functionalized with PI4P phosphatase Sac1p and phosphatidylinositol (PI) 4-kinase, respectively. Using real-time assays, we demonstrate that upon adenosine triphosphate (ATP) addition, Osh4p creates a sterol gradient between these membranes, relying on the spatially distant synthesis and hydrolysis of PI4P, and quantify how much PI4P is needed for this process. Then, we develop a quantitatively accurate kinetic model, validated by our data, and extrapolate this to estimate to what extent PI4P metabolism can drive ORP-mediated sterol transfer in cells. Finally, we show that Sec14p can support PI4P metabolism and Osh4p activity by transferring PI between membranes. This study establishes that PI4P synthesis drives ORP-mediated lipid exchange and that ATP energy is needed to generate intermembrane lipid gradients. Furthermore, it defines to what extent ORPs can distribute lipids in the cell and reassesses the role of PI-transfer proteins in PI4P metabolism.

lipid transfer protein | sterol | phosphatidylinositol 4-phosphate | ATP | lipid gradient

Significance

OSBP (oxysterol-binding protein)-related proteins (ORPs) are critical in lipid distribution within eukaryotic cells. They transfer sterol or phosphatidylserine (PS) from the ER (endoplasmic reticulum) to other subcellular regions by exchanging them for another lipid, PI4P. However, whether the synthesis and hydrolysis of PI4P, which pilot these exchanges, guarantee substantial intracellular sterol and PS fluxes is unclear. To address this question, difficult to tackle quantitatively in situ, we have developed sophisticated assays using purified proteins and artificial membranes to analyze the coupling between ORPs activity and PI4P metabolism at the ER/Golgi interface. Next, using a mathematical model, we define how this coupling contributes to intracellular lipid distribution. Finally, we show that Sec14-mediated intermembrane phosphatidylinositol transfer mediated promotes PI4P synthesis and ORP activity.

Lipids are precisely distributed among the organelles and the plasma membrane (PM) of eukaryotic cells, which is critical for cellular architecture and functions such as vesicular trafficking or signal transduction (1, 2). This distribution relies on lipid transfer proteins (LTPs) that carry lipids, across the cytosol, between membranes in which these lipids are enzymatically produced or modified. OSBP (Oxysterol-binding protein) and several OSBP-related proteins (ORPs) in human cells [oxysterol-binding homology (Osh) proteins in yeast] are LTPs involved in the intracellular distribution of sterols (cholesterol in human cells and ergosterol in yeast) and phosphatidylserine (PS), accounting for 12 to 20% and 2 to 10% of cell lipids, respectively (3, 4). These lipids are produced in the ER (endoplasmic reticulum) but are essentially found in the *trans*-Golgi and the PM (5–8), where they play vital roles. Sterol guarantees the rigidity and inner organization of these membranes (5, 6), whereas PS, an anionic phospholipid, contributes to recruiting signaling proteins on the inner leaflet of the PM via electrostatic interactions (7, 8). This asymmetrical distribution of sterol and PS can be established by ORPs coupled to the metabolism of PI4P, a lipid belonging to the phosphoinositide class, but to a degree that remains ill-defined (9).

ORPs have various molecular organizations, but all comprise an OSBP-related domain (ORD) with a lipid-binding pocket (10). As first identified with Osh4p and OSBP (11, 12), some of these can host a molecule of sterol and PI4P alternatively and exchange these lipids between membranes (10). Others, like Osh6p and Osh7p and their closest homologues ORP5 and ORP8, act as PS/PI4P exchangers (13, 14). A general model assumes that ORPs extract sterol or PS from the ER and exchange these lipids with PI4P on the *trans*-Golgi and PM in which this lipid is produced by PI 4-kinases through the phosphorylation of phosphatidylinositol (PI). Then, ORPs transfer PI4P to the ER membrane, where PI4P is hydrolyzed by the phosphatase Sac1. The constant synthesis and hydrolysis of PI4P drive continuous exchange cycles, leading to the build-up of sterol and PS in the *trans*-Golgi and/or PM at the expense of the ER, thereby creating asymmetry (9, 10).

Many observations support this model. For instance, in vitro studies have shown that Osh4p can vectorially transfer sterol between two membranes using a preexisting PI4P gradient (15). In yeast, Osh2p supplies the PM with ergosterol unless it cannot trap PI4P (16). Osh6p transfers PS from the ER to the PM unless Sac1p is silenced, which suggests that its activity is driven by a PI4P gradient between these two membranes (13). ORP5 and ORP8 depend similarly on PI4P (14). Solid evidence also indicates that OSBP supplies the *trans*-Golgi with sterol owing to a PI4P gradient at the ER/Golgi interface (12, 17).

Author contributions: A.S. and G.D. designed research; N.F., M.M., A.H., and G.D. performed research; N.R. and A.S. developed kinetic models; N.F., N.R., M.M., A.S., and G.D. analyzed data; A.S. and G.D. funding; and N.R., A.S., and G.D. wrote the paper.

The authors declare no competing interest.

This article is a PNAS Direct Submission.

Copyright © 2024 the Author(s). Published by PNAS. This article is distributed under Creative Commons Attribution-NonCommercial-NoDerivatives License 4.0 (CC BY-NC-ND).

[1]N.F., N.R., and M.M. contributed equally to this work.

[2]To whom correspondence may be addressed. Email: agnese.seminara@unige.it or drin@ipmc.cnrs.fr.

This article contains supporting information online at https://www.pnas.org/lookup/suppl/doi:10.1073/pnas.2315493121/-/DCSupplemental.

Published February 26, 2024.

Downloaded from https://www.pnas.org by 88.122.22.207 on November 5, 2024 from IP address 88.122.22.207.

Moreover, various ORPs seem capable of transferring sterol and PS to endosomes and lysosomes in which PI4P is also present (18–20). Nevertheless, it has not been directly demonstrated that PI4P synthesis drives the exchange activity of ORPs.

Furthermore, it is unclear whether ORPs carry sterol and PS massively throughout the cell or only fine-tune organelle lipid composition (9). For instance, OSBP seems to transfer a considerable amount of sterol to the Golgi (12, 17) but also to control protein recycling at the endosomal level through a fine regulation of PI4P (21). In yeast cells, Osh4p might deliver sterol to the *trans*-Golgi to promote the formation of secretory vesicles (22), but data suggest that its only role would be to guarantee the docking of these vesicles to the PM by extracting PI4P (23, 24). It is also assumed that ORP5 and ORP8 do not deliver high quantities of PS to the PM but only adjust the level of PS, PI4P, and another phosphoinositide, $PI(4,5)P_2$, in this membrane (25).

The cellular role of ORPs remains difficult to ascertain because it is unclear to what extent PI4P metabolism can drive their activities. The exchange model posits that one molecule of PI4P is used to transfer one molecule of counterligand. But PI4P is found in trace amounts in the cells [in yeast, only 0.2% of lipids (26)] compared to sterol and PS, which seems incompatible with the implementation of intensive lipid exchange. Nevertheless, in yeast lacking Sac1p or all Osh proteins, PI4P levels can be multiplied by up to ~20 (27, 28), which suggests that PI4P pools, possibly accounting for 2 to 4% of total phospholipids (22), are constantly synthesized and hydrolyzed to support Osh activities. Also, OSBP has been shown to use half of PI4P produced in human cells to guarantee 30 to 60% of ER-to-Golgi sterol transfer (17). Yet, apart from these data, we have no quantitative insights into the coupling between ORP-mediated lipid exchange and PI4P metabolism.

Because the activity of ORPs depends on PI4P, this also raises the question of how the availability of PI is maintained in the cytosolic leaflet of the endosomal, Golgi, and plasma membranes PM abbrevation cannot be used here because we refer to three membranes (endosome membrane, Golgi membrane and plasma membrane)to guarantee PI4P synthesis (29, 30). So far, little is known about how PI is exported to other organelles from the ER, where it is made. In yeast, Sec14p supports the production of PI4P in the Golgi by the PI 4-kinase Pik1p and the secretory function of this organelle (26, 31, 32), possibly by transferring PI from the ER via PI/phosphatidylcholine (PC) exchange, yet this model is disputed (33). Intriguingly, Sac1p and Osh4p counteract Sec14p and Pik1p functions (32, 34–36). In human cells, a distinct class of PI-transfer proteins is thought to regulate the level of PI4P and other phosphoinositides in the Golgi and PM (33, 37). Moreover, a few clues suggest that some of these support the activity of OSBP (38, 39). Likely, PI-transfer proteins are functionally linked to PI4P metabolism and ORP-mediated lipid exchange.

To better define the couplings between ORPs activities, PI4P metabolism, and PI-transfer processes, we reconstituted an ER/Golgi interface in vitro with liposomes covered by Sac1p and liposomes functionalized with a PI 4-kinase. Using real-time assays, we established that Osh4p could create a sterol gradient between these membranes when PI4P was synthesized upon ATP addition, and we determined the amount of PI4P and ATP needed for this process. Then, we built a mathematical model, validated by our data, to define whether cellular PI4P metabolism could pilot substantial ORP-mediated sterol transfer. Finally, we showed that Sec14p, by transferring PI between membranes, could support the synthesis of PI4P and Osh4p-mediated sterol transfer. This study establishes that PI4P metabolism can drive ORP-mediated lipid transfer and that ATP is needed to build lipid gradients between membranes. Furthermore, it defines more precisely to what extent ORPs can distribute lipids in the cell and the role of PI-transfer proteins in PI4P metabolism.

Results

PI4P Synthesis on PI-Rich Liposomes by a Membrane-Bound PI 4-Kinase. To reconstitute an ER/Golgi interface, an essential step was to anchor Sac1 and a PI 4-kinase to distinct membranes. We had already obtained a Sac1p[1–522]His_6 construct that could be attached to liposomes doped with 1,2-dioleoyl-*sn*-glycero-3-[(N-(5-amino-1-carboxypentyl)iminodiacetic acid)succinyl] (nickel salt) (DOGS-NTA-Ni^{2+}), via a C-terminal His-tag that substitutes for the transmembrane segment of this protein (15). So, we focused on the design of a PI 4-kinase that could be attached to liposomes using a different strategy. To achieve this, we re-engineered a catalytically active fragment of the PI 4-kinase IIα (PI4KIIα^{SSPSS}ΔC, segment 78 to 453) in which the cysteine residues of the ^{174}CCPCC^{178} motif, which are palmitoylated to anchor the protein to the membrane, had been replaced by serine residues (40). We reintroduced one cysteine in this motif (C178) and replaced three endogenous cysteine residues exposed at the protein surface with serine residues. Our idea was to covalently attach this kinase via the C178 cysteine to the surface of liposomes containing the thiol-reactive 1,2-dioleoyl-*sn*-glycero-3-phosphoethanolamine-N-[4-(p-maleimidophenyl) butyramide] (MPB-PE) lipid, with a proper orientation allowing the phosphorylation of the PI headgroup (Fig. 1*A*). This construct (called PI4K), purified in the presence of DTT (*SI Appendix*, Fig. S1), was applied to a desalting column to remove DTT and incubated (at 4 μM) for 1 h with liposomes (800 μM lipids) only composed of 1,2-dioleoyl-*sn*-glycero-3-phosphocholine (DOPC) or additionally containing 3% MPB-PE, 10% PI or both lipids. Using flotation assays (Fig. 1*B*), we found that PI4K was weakly associated with pure DOPC liposomes (5% of total protein) but seven times more with MPB-PE-containing liposomes, which suggested that the protein was covalently attached to the latter. PI4K was slightly bound (10%) to liposomes doped with PI, possibly through specific recognition of PI and/or nonspecific electrostatic interaction. Finally, the highest binding (60%) was measured with liposomes containing PI and MPB-PE. These data suggested that PI4K could be efficiently anchored to PI-rich liposomes.

We then tested whether the kinase, attached to liposomes, synthesized PI4P in the presence of ATP (Fig. 1*C*). To this end, we followed in real-time the formation of PI4P in the outer leaflet of these liposomes using NBD-PH_{FAPP}, a specific fluorescent sensor; when this construct docks onto a membrane upon interacting with PI4P, its fluorescence increases because the NBD fluorophore shifts from a polar to a hydrophobic environment (13, 15). Liposomes composed of DOPC/PI/MPB-PE (87/10/3) were incubated with PI4K for 1 h to be functionalized with the kinase and diluted in a cuvette thermostated at 30 °C. The final concentrations were 1 μM PI4K and 200 μM lipids (PI4K/L molar ratio = 1/100 considering only accessible lipids). NBD-PH_{FAPP} was added, resulting in a signal jump at 525 nm (excitation at 495 nm). Five minutes later, ATP was injected (100 μM final concentration), which elicited a rapid increase in fluorescence, indicating the progressive recruitment of NBD-PH_{FAPP} on liposomes (Fig. 1*D*). A plateau was reached within 1 h. If the kinase was incubated with liposomes containing PI but not MPB-PE, the increase in NBD signal was much lower, whereas with liposomes devoid of PI or kinase, a very slight or no increase was observed, respectively. Jointly, these data suggested that PI4K, when covalently attached to PI-rich liposomes, generated PI4P.

We performed further experiments with PI-rich liposomes functionalized with PI4K in the absence or presence of 200 μM

Downloaded from https://www.pnas.org by 88.122.22.207 on November 5, 2024 from IP address 88.122.22.207.

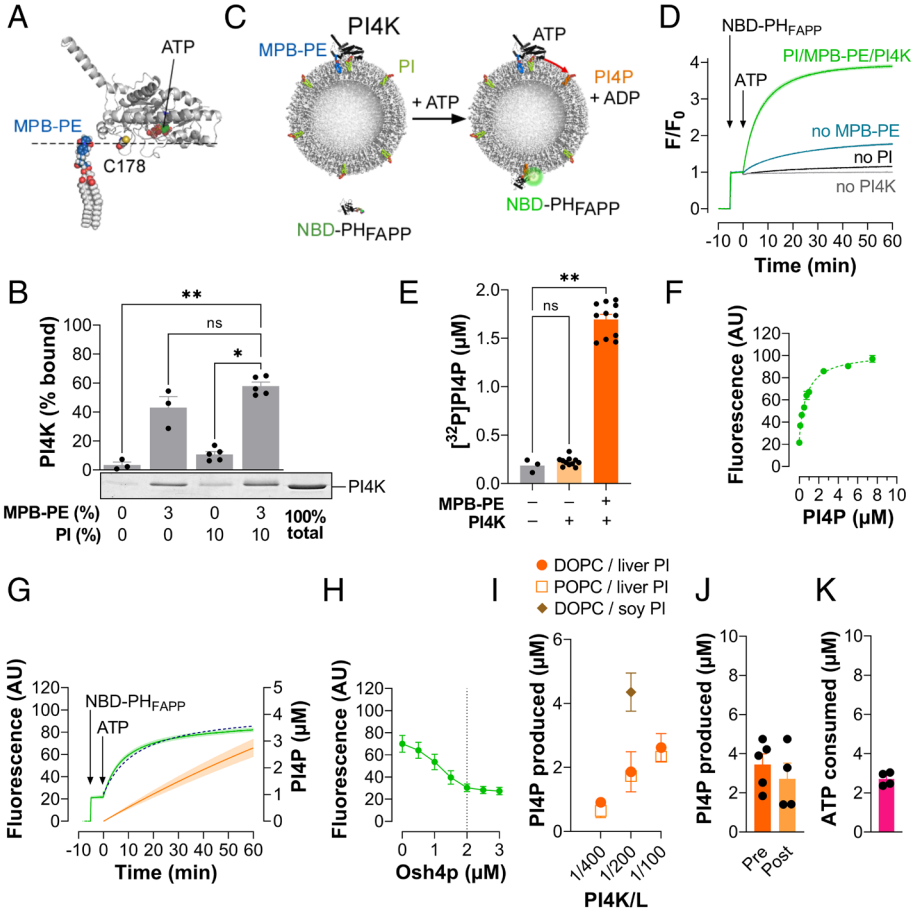

Fig. 1. PI4P synthesis on the liposome surface by membrane-associated PI 4-kinase. (*A*) Structure of PI4KIIα^{SSPSS}ΔC in complex with an ATP molecule (PDB ID: 4HNE; ATP is represented in sphere mode, with carbon in green, nitrogen in blue, oxygen in red, and phosphorus in orange). A serine residue (S178) in the SSPSS sequence was replaced by a cysteine residue (represented in sphere mode, carbon in gray, sulfur in yellow). The orientation of the kinase relative to the membrane surface (dashed line) was suggested by molecular dynamics simulations (40). A molecule of MPB-PE is represented with carbon in gray (glycerol and acyl chain) or dark blue (headgroup), oxygen in red, nitrogen in blue, phosphorus in orange, and hydrogen in white. The figure was prepared using PyMOL (http://pymol.org/). (*B*) Flotation assays. PI4K (4 μM) was mixed with liposomes (800 μM lipids) only made of DOPC or containing 10% liver PI, 3% MPB-PE, or both lipids in HK buffer at 25 °C for 1 h. The functionalization reaction was stopped by adding 1 mM DTT. After centrifugation, the liposomes were recovered at the top of sucrose cushions and analyzed by sodium dodecyl-sulfate polyacrylamide gel electrophoresis (SDS-PAGE). The amount of membrane-bound PI4K was determined using the content of lane 5 (100% total) as a reference based on the SYPRO Orange signal. Data are represented as mean ± SEM (n = 3 to 5) with single data points. Kruskal–Wallis with Dunn's multiple comparison test (*P < 0.05 and **P < 0.01). (*C*) Principle of PI4P detection in the membrane coated with PI4K using NBD-PH$_{FAPP}$. ATP is added to PI-containing liposomes functionalized with PI4K. If PI4P is synthesized, NBD-PH$_{FAPP}$ binds to the liposomes and becomes more fluorescent. (*D*) Liposomes (800 μM) composed of DOPC/liver PI/MPB-PE (87/10/3) were mixed for 1 h with 4 μM of DTT-free PI4K (PI4K/L molar ratio = 1/100 considering only lipids in the outer leaflet). This mixture was diluted fourfold in 600 μL HK buffer containing 7 mM $MgCl_2$ (HKM7 buffer). Then, NBD-PH$_{FAPP}$ (250 nM) and ATP (100 μM) were sequentially injected. Control experiments were conducted without PI4K or with liposomes devoid of MPB-PE or PI. The signal was measured at λ = 525 nm (λ_{ex} = 495 nm). The fluorescence was normalized to the F_0 fluorescence recorded before the last injection. Each trace is the mean ± SEM of kinetics recorded in independent assays (green trace, PI-containing liposomes coated with PI4K, n = 4; blue-green trace, liposomes without MPB-PE, n = 3; black trace, PI-free liposomes, n = 3; gray trace, without PI4K, n = 4). (*E*) Kinase assay. [γ-^{32}P]ATP (100 μM) was added to DOPC liposomes (200 μM) containing 10% PI, with or without 3% MPB-PE, and preincubated for 1 h with PI4K (PI4K/L = 1/200). Control experiments were conducted with PI-containing liposomes alone. The reaction was allowed to proceed for 1 h at 30 °C under agitation. The lipids were extracted and dried. The radioactivity in the reaction mix and associated with lipids was counted to quantify newly made PI4P. Orange bars, with MPB-PE-containing liposomes; light-orange bars, with MPB-PE-free liposomes; gray bars, without PI4K. Data are represented as mean ± SEM (n = 3 to 11). Kruskal–Wallis with Dunn's multiple comparison test; **P < 0.01, ns: $P \geq 0.05$. (*F*) Fluorescence of NBD-PH$_{FAPP}$ (250 nM) incubated with liposomes (200 μM) made of DOPC and containing increasing amounts of PI4P at the expense of PI [with PI + PI4P accounting for 10% of lipids]. The intensity F is given as a function of the volume concentration of PI4P, resulting in a binding curve that can be fitted considering $F = F_0 + F_B \times [PI4P]/([PI4P] + K_D)$ and a 1:1 stoichiometry. (*G*) Determination of PI4P production. Liposomes (800 μM), composed of DOPC/liver PI/MPB-PE (87/10/3) and functionalized with PI4K (PI4K/L= 1/100), were diluted fourfold in HKM7 buffer. Then, NBD-PH$_{FAPP}$ (250 nM) and ATP were added. The fluorescence signal was measured at 525 nm (λ_{ex} = 495 nm, green trace) and corrected for photobleaching. The data points were fitted (dotted curve, considering a pseudo-first-order reaction) to determine the rate of PI4P synthesis and calculate the amount of PI4P produced over time (orange curve, *SI Appendix*). Mean ± SEM (n = 3 to 4). (*H*) Incremental amounts of Osh4p were added to liposomes at the end of kinetics shown in (*G*). A minimal signal was reached once 2.5 to 3 μM Osh4p was added (dashed lines), suggesting that a similar amount of PI4P was present in the outer leaflet of liposomes and extracted by the protein. (*I*) Amount of PI4P synthesized after 1 h in DOPC or POPC membranes enriched with 10% liver PI (mostly 18:0/20:4-PI) or soy PI (mostly 16:0/18:2-PI) and functionalized with a variable quantity of PI4K. Mean ± SEM (n = 3 to 5). (*J*) Amount of PI4P produced in PI-containing membranes functionalized with PI4K within 1 h following ATP addition estimated by fitting the kinetics traces shown in *SI Appendix*, Fig. S3*C* (orange bars, nonisolated liposomes; light-orange bars, isolated liposomes). Mean ± SEM (n = 4 to 5). (*K*) Amount of ATP hydrolyzed in 1 h by PI4K at the surface of PI-containing liposomes used for assays shown in *SI Appendix*, Fig. S3*C*. Mean ± SEM (n = 4).

adenosine, an inhibitor of class II PI 4-kinases (41). As shown in *SI Appendix*, Fig. S2*A*, the signal increased more slowly in the presence of adenosine, which confirmed that we were measuring a kinase-dependent PI4P synthesis process. Finally, we measured the production of PI4P using an alternative, radioactivity-based assay adapted from (42). PI-containing liposomes, doped or not with MPB-PE, were incubated with PI4K for 1 h and then mixed with [γ-^{32}P]ATP for an extra hour at 30 °C. Control experiments with PI-containing liposomes only were conducted. After liquid extraction, the amount of radioactivity incorporated in organic

Downloaded from https://www.pnas.org by 88.122.22.207 on November 5, 2024 from IP address 88.122.22.207.

solvent-extractable material, resulting from the phosphorylation of PI, was counted. A significant level of radioactivity, corresponding to the production of ~ 2 μM PI4P, was measured only if PI4K was present and covalently attached to liposomes via MPB-PE (Fig. 1*E*). These data confirmed that the membrane-bound form of PI4K produced PI4P.

Quantification of PI4P Generated by the PI 4-Kinase on the Liposome Surface. Next, we estimated how much PI4P was synthesized by PI4K based on our assay using NBD-PH_{FAPP}. The increase in the signal cannot linearly follow the amount of PI4P that is synthesized because it depends on a 1:1 binding process between NBD-PH_{FAPP} and PI4P that is governed by the affinity of the sensor for its ligand. Thus, to interpret our kinetics, we measured in separate experiments the fluorescence of NBD-PH_{FAPP} in the presence of different liposomes each with a composition corresponding to a given degree of PI-to-PI4P conversion: The fraction of PI4P ranged from 0 to 7.5% of lipids at the expense of PI (so that PI and PI4P always represented a total of 10% as in the kinase assays). The fluorescence was recorded with measurement settings identical to those used to follow PI4P synthesis. By plotting the intensity of the NBD signal as a function of PI4P concentration, we obtained a binding curve that could be fitted assuming a 1:1 protein-ligand interaction model (Fig. 1*F*). Then, using the parameters obtained (F_0, F_B, and K_D) and considering that PI-to-PI4P conversion occurred following a pseudo-first-order reaction, we fitted the data points of kinetics traces obtained with NBD-PH_{FAPP}, to estimate how much PI4P was synthesized over time (*SI Appendix*). In assays with liposomes (200 μM lipids, 10 μM accessible PI), coated with 0.25, 0.5 or 1 μM PI4K, we measured that the rate of PI4P synthesis was proportional to the surface density of kinase, with a maximum of 2.6 ± 0.4 μM PI4P synthesized in 1 h at PI4K/L = 1/100 (n = 4, ± SEM, Fig. 1 *G* and *I* and *SI Appendix*, Fig. S2*B*). ORPs can extract PI4P from the membrane with a 1:1 stoichiometry (13, 15) and can be used to estimate how much of this lipid is present in a membrane. Therefore, at the end of measurements conducted at PI4K/L = 1/100, we added incremental amounts of Osh4p and observed that the NBD signal returned to its initial level once Osh4p concentration reached 2.5 to 3 μM (Fig. 1*H*). This suggested that a corresponding amount of PI4P was in the membrane and had been extracted by Osh4p, confirming our evaluation of PI4P production from kinetic traces.

Next, we examined whether PI4K activity could be influenced by the fluidity of the membrane, given that PI4KIIα might be sensitive to this factor (40), using functionalized liposomes composed of POPC instead of DOPC, doped with PI. We estimated that the PI4P production was not greater (Fig. 1*I* and *SI Appendix*, Fig. S2 *C* and *D*). In contrast, we observed that PI4P was produced faster when liver PI was replaced by soy PI for the same amount of PI4K (Fig. 1*I* and *SI Appendix*, Fig. S2 *E* and *F*), possibly because the acyl chains of these PI species differ (16:0/18:2 vs. 18:0/20:4). This observation allowed us to use less PI4K to produce PI4P in some of our following assays.

Furthermore, we characterized PI4K by quantifying how much it hydrolyzed ATP when synthesizing PI4P. First assays showed that ATP was hydrolyzed even when PI4K was mixed with liposomes devoid of PI, possibly due to minute amounts of contaminants in the kinase preparation (e.g., *Escherichia coli* chaperones). We then decided to prepare PI-containing liposomes, doped or not with MPB-PE, mixed with PI4K, and to separate them from potential contaminants at the top of sucrose cushions. SDS-PAGE analyses and intrinsic fluorescence measurements, conducted with the same liposomes, subjected or not to this flotation assay (pre/post), confirmed that only isolated liposomes doped with MPB-PE were substantially covered with PI4K (80% of total protein, *SI Appendix*, Fig. S3 *A* and *B*). Then, with these liposomes, we measured that 2.7 μM PI4P were produced by PI4K in 1 h following ATP addition (Fig. 1*J* and *SI Appendix*, Fig. S3*C*), slightly less than the amount measured with the same liposomes, not subjected to the flotation assay (3.5 μM). Comparatively, almost no PI4P was produced with nonfunctionalized liposomes (*SI Appendix*, Fig. S3*C*). Finally, using a standard luminescence-based assay, we measured the amount of ATP hydrolyzed in samples of isolated liposomes in conditions identical to those used to measure PI4P synthesis (*SI Appendix*, Fig. S3*D*). By subtracting the values obtained with liposomes devoid of attached PI4K from those obtained with functionalized liposomes, we estimated that the kinase specifically hydrolyzed 2.7 ± 0.2 ATP molecules in 1 h (Fig. 1*K*). These data, compared to those obtained on PI4P synthesis, suggest that ~1 molecule of ATP is used by PI4K to produce 1 molecule of PI4P, hence, that PI4P synthesis occurs with no ATP-consuming futile cycle.

PI4P Synthesis and Hydrolysis Allow Osh4p to Create a Sterol Gradient between Membranes. Once PI4K activity was characterized, we set up a complete system mimicking the ER/Golgi interface to measure the sterol/PI4P exchange activity of Osh4p driven by PI4P metabolism. As a first step, we assessed whether Osh4p could transfer PI4P synthesized by PI4K bound to PI-rich liposomes (Golgi mimetic, termed L_G) to liposomes only made of DOPC (ER mimetic, L_E). Equivalent amounts of these liposomes (200 μM lipids each) were mixed with NBD-PH_{FAPP}. Importantly, for this assay, L_G liposomes were also doped with 2% 1,2-dipalmitoyl-*sn*-glycero-3-phosphoethanolamine-N-(lissamine rhodamine B sulfonyl) (Rhod-PE). We reasoned that the production of PI4P would trigger the association of NBD-PH_{FAPP} to L_G liposomes, but the presence of Rhod-PE would quench the fluorescence of the sensor by FRET. However, we expected that if Osh4p subsequently transported PI4P to L_E liposomes, this would cause the translocation of NBD-PH_{FAPP} onto membranes devoid of Rhod-PE and, consequently, an increase in fluorescence (Fig. 2*A*). As expected, when ATP alone was added to liposomes, the signal of the sensor remained unchanged. In contrast, when ATP and Osh4p (200 nM) were added together, the NBD signal progressively increased, suggesting that once PI4P was synthesized in L_G membranes, it was transferred to L_E membranes (Fig. 2*A*). We repeated this experiment with L_E liposomes containing 2.5% of dehydroergosterol (DHE), which is a perfect ergosterol mimetic recognized by Osh4p (11, 15). The NBD signal increased more rapidly, suggesting that PI4P was delivered much faster to L_E liposomes. This acceleration seen within the first seconds is explained by the fact that Osh4p can exchange PI4P for DHE (15). These data indicated that PI4P generated by PI4K in L_G liposomes could be transferred by Osh4p to L_E liposomes and exchanged with sterol contained in these latter.

Next, we modified our system to measure whether Osh4p could transfer sterol from L_E to L_G membranes in the presence of a PI4P gradient generated between these membranes by PI4K and Sac1p (Fig. 2*B*). We prepared L_E liposomes including 2% DOGS-NTA-Ni^{2+} to be functionalized with Sac1p[1–522]His_6. Using flotation assays, we checked that when these liposomes were mixed with L_G liposomes coated with PI4K, no exchange of proteins between the two types of liposomes occurred (*SI Appendix*, Fig. S4 *A* and *B*). This indicated that the spatial separation of PI4K and Sac1p, necessary for creating an intermembrane PI4P gradient, could be maintained over time. Then, we measured sterol transfer using L_E liposomes that additionally contained 2.5% DHE and DNS-PE [1,2-dioleoyl-*sn*-glycero-3-phosphoethanolamine-N-(5-dimethylamino-1-naphthalenesulfonyl)], functionalized with

Downloaded from https://www.pnas.org by 88.122.22.207 on November 5, 2024 from IP address 88.122.22.207.

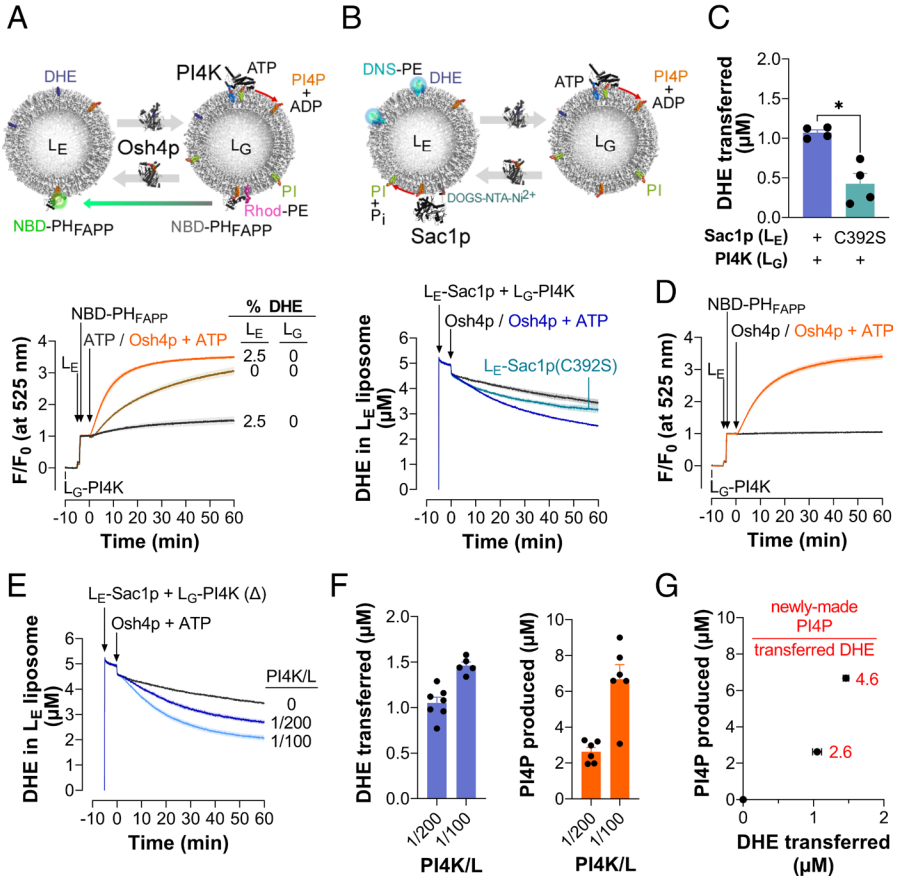

Fig. 2. PI4P synthesis and hydrolysis drive sterol transfer by Osh4p between membranes. (*A*) Osh4p-mediated PI4P transfer coupled to PI4P synthesis. L_E liposomes (200 μM) only made of DOPC or additionally containing 2.5% DHE, were added to an equal amount of L_G liposomes composed of DOPC/liver PI/MPB-PE/Rhod-PE (85/10/3/2) and functionalized with PI4K (at PI4K/lipid = 1/100). One minute later, NBD-PH_{FAPP} (250 nM) was added. After a 5-min incubation, ATP only or together with Osh4p (200 nM) was injected. Fluorescence was measured at 525 nm (λ_{ex} = 460 nm). Mean ± SEM. (gray trace, ATP without Osh4p, n = 3; brown and orange trace, ATP premixed with Osh4p, n = 3 to 4). (*B*) Osh4p-mediated DHE transfer driven by a PI4P gradient generated by PI4K and Sac1p. L_E liposomes (200 μM), composed of DOPC/DHE/DNS-PE/DOGS-NTA-Ni^{2+} (93/2.5/2.5/2), and covered with Sac1p[1-522]His_6 or its C392S inactive form (100 nM), were added to an equal amount of L_G liposomes composed of DOPC/liver PI/MPB-PE/DHE (84.5/10/3/2.5) and functionalized with PI4K (PI4K/L = 1/100). Five minutes later, 200 nM Osh4p, alone or together with ATP, were injected. Fluorescence was recorded at 525 nm (λ_{ex} = 310 nm) and normalized in terms of DHE present in L_E liposomes. Mean ± SEM. (gray trace, Osh4p without ATP, L_E liposomes coated with Sac1p[1-522]His_6, n = 4; blue trace, Osh4p premixed with ATP, L_E liposomes coated with Sac1p[1-522]His_6, n = 4; blue-green trace, Osh4p premixed with ATP, L_E liposomes with Sac1p[1-522]His_6(C392S), n = 4). (*C*) Amount of DHE specifically transferred by Osh4p from L_E liposomes, coated with Sac1p (blue bar) or its inactive C392S form (green bar), to L_G liposomes covered with PI4K within 1 h in the presence of ATP. Data are represented as mean ± SEM (n = 4). Unpaired Mann–Whitney *U* test; *$P < 0.05$. (D) PI4P-transport coupled to PI4P synthesis between L_E and L_G liposomes, both containing 2.5% DHE. L_G liposomes (200 μM) composed of DOPC/liver PI/MPB-PE/DHE/Rhod-PE (82.5/10/3/2.5/2) and functionalized with PI4K (PI4K/L = 1/100) were mixed with an equal amount of L_E liposomes, composed of DOPC/DHE (97.5/2.5). NBD-PH_{FAPP} was added, followed by the injection of Osh4p, alone or with ATP. Fluorescence was measured at 525 nm (λ_{ex} = 460 nm). Mean ± SEM (gray trace, Osh4p without ATP, n = 3; orange trace, Osh4p premixed with ATP, n = 4). (*E*) Osh4p-mediated DHE transfer as a function of PI4K density on L_G liposomes. L_E liposomes composed of DOPC/DHE/DNS-PE/DOGS-NTA-Ni^{2+} (93/2.5/2.5/2) covered with Sac1p[1-522]His_6 were added to L_G liposomes composed of DOPC/soy PI/MPB-PE/DHE (84.5/10/3/2.5) and functionalized with different amounts of PI4K (PI4K/L = 0, 1/100 or 1/200). After 5 min, Osh4p and ATP were injected. Mean ± SEM (n = 6 to 7). (*F*) Amount of DHE transferred by Osh4p from L_E to L_G liposomes and amount of PI4P produced in L_G liposomes in 1 h, as a function of the quantity of PI4K used to functionalize L_G membranes, determined from curves shown in *SI Appendix*, Fig. S5*A*. Mean ± SEM (n = 6). (*G*) Amount of Osh4p-mediated DHE transfer as a function of PI4P synthesized in L_G membranes by PI4K. Mean ± SEM.

Sac1p (100 nM) or its catalytically dead version (C392S). In parallel, we prepared L_G liposomes containing 2.5% DHE and 10% PI, covered by PI4K, whose activity was checked (*SI Appendix*, Fig. S4*C*). Equivalent amounts of L_E and L_G liposomes (200 μM lipids each) were mixed, and the FRET signal between DHE and DNS-PE contained in the L_E membranes was measured. Adding Osh4p alone (200 nM) to liposomes only caused a slight drop in signal followed by a slow decrease that was identical to that measured before injecting the protein, likely due to photobleaching (Fig. 2*B*, gray trace). This suggested that Osh4p only extracted a stoichiometric amount of DHE from L_E liposomes with no transfer to L_G liposomes. In contrast, when ATP was added to trigger PI4P synthesis, along with Osh4p, a faster decrease in signal was observed, indicating that Osh4p delivered sterol to L_G liposomes (Fig. 2*B*, blue trace). Importantly, given that DHE was initially equally distributed between membranes, this meant that Osh4p could create a sterol gradient as PI4P was synthesized. Moreover, when L_E liposomes were coated with active Sac1p, we observed that the amount of transferred DHE after 1 h was higher than that measured using L_E liposomes coated with a catalytically dead phosphatase (1.1 μM vs. 0.42 μM, Fig. 2 *B* and *C*). These data indicated that the production of PI4P alone could drive the creation of a sterol gradient by Osh4p between the two membranes and that its hydrolysis on the ER-mimetic membrane improved this process.

Additional data confirmed that Osh4p carried sterol from the ER- to the Golgi-mimetic membranes by transporting newly made PI4P in the opposite direction. First, using NBD-PH_{FAPP}, we

Downloaded from https://www.pnas.org by 88.122.22.207 on November 5, 2024 from IP address 88.122.22.207.

measured that Osh4p transferred PI4P, synthesized in L_G liposomes in the presence of ATP, to L_E liposomes (covered by inactive Sac1p so that PI4P was detectable), with both types of liposomes initially containing 2.5% DHE as in the DHE transfer assays (Fig. 2*D*). Second, we repeated the DHE and PI4P transfer experiments with an Osh4p(H143A/H144A) mutant deficient in binding PI4P (11, 15) and found that it was unable to transfer sterol and PI4P between membranes when PI4P was synthesized (*SI Appendix*, Fig. S4*D*). These results showed that the exchange activity of Osh4p was coupled to PI4P metabolism in our artificial ER/Golgi interface. Therefore, we fully demonstrate that upon ATP addition, a PI 4-kinase and PI4P phosphatase on two distinct membranes can drive the exchange activity of an ORP and the creation of a lipid gradient between these membranes.

Relationship between ATP-Dependent PI4P Synthesis and Sterol Transfer. Next, we quantified how much PI4P was necessary to allow for the creation by Osh4p of a sterol gradient between membranes using L_E and L_G liposomes initially containing the same amount of DHE, as done for assays shown in Fig. 2*B*. L_G liposomes containing 10% soy PI and 2.5% DHE were functionalized with two different concentrations of PI4K (PI4K/L = 1/100 or 1/200). Then, for each L_G liposome batch, we performed two parallel measurements in similar conditions in the presence of ATP. First, we determined how much PI4P was produced by PI4K in 1 h using the NBD-PH_{FAPP} sensor. Second, we measured how much DHE was transferred by Osh4p from L_E liposomes, containing 2.5% DHE and covered by Sac1p, to the L_G liposomes over the same period; control experiments were carried out with L_G liposomes devoid of kinase. We found that the production of PI4P was higher if L_G liposomes were functionalized with a higher density of PI4K (*SI Appendix*, Fig. S5*A*) and concomitantly, that Osh4p transferred more DHE to these liposomes (Fig. 2*E*). We established that the synthesis of 2.6 and 6.7 μM PI4P drove the transfer of 1 and 1.5 μM DHE respectively (Fig. 2*F*). This indicated that the transfer of one molecule of DHE during the creation of a sterol gradient required the synthesis of more than one PI4P molecule (Fig. 2*G*). This also indicated that for the generation of a steeper sterol gradient, a higher production of PI4P was needed for the transfer of a similar DHE amount. Overall, these data suggested that the creation of a sterol gradient did not simply result from a one-for-one exchange of sterol and PI4P in our system.

To better analyze this, we tested whether a preestablished DHE gradient between L_E and L_G membranes could be dissipated through spontaneous DHE transfer in the timescale of our assays. We mixed L_E liposomes containing 1.5 or 0.5% DHE with L_G liposomes containing 3.5 or 4.5% DHE, respectively, in the absence of protein and measured a substantial transfer of DHE from L_G to L_E liposomes in 1 h (up to 1.6 μM DHE with the steepest gradient, *SI Appendix*, Fig. S5*B*). Thus, if the creation of a sterol gradient by Osh4p required a PI4P amount higher than expected, this was likely because spontaneous DHE transfer counteracted the creation of this gradient.

To extend our analyses, we estimated how much ATP was hydrolyzed by the kinase to drive sterol transfer by Osh4p. To do so, we conducted DHE transfer and ATP hydrolysis assays using L_G liposomes, functionalized or not with PI4K (–/+MPB-PE) and isolated on sucrose cushions (*SI Appendix*, Fig. S5*C*). We determined that ~1 μM of DHE was specifically transported in 1 h from L_E liposomes to L_G liposomes functionalized with PI4K and that ~2.6 μM of ATP were hydrolyzed at the surface of these liposomes over the same period (*SI Appendix*, Fig. S5 *D* and *E*). The latter value matched the amount of PI4P that had to be synthesized to transfer 1 μM DHE in the same condition (Fig. 2*F*). We concluded that the amounts of hydrolyzed ATP and newly made PI4P necessary for the transfer of a given amount of DHE by Osh4p were similar, corroborating our observations that PI4K uses one ATP molecule to produce one PI4P molecule (Fig. 1 *J* and *K*).

Kinetic Model of Osh4p-Mediated Sterol/PI4P Exchange Powered by PI4P Metabolism. Next, to analyze our data, we developed a kinetic model that describes PI4P synthesis and hydrolysis as well as the Osh4p-mediated sterol and PI4P transport in our system. We modeled changes in six concentrations: PI4P in L_E membranes (p_E), in L_G membranes (p_G) and in complexes with Osh4p (p_o), and similarly for sterol (s_E, s_G, and s_o, Fig. 3*A*). We wrote six nonlinear kinetic equations with a specific form justified experimentally (*SI Appendix*, Eq. **S7**). In our DHE-transfer assays, all Osh4p proteins were initially preloaded with sterol, hence $s_o = O$ (Osh4p concentration) and $p_o = 0$. We numerically integrated the full system using $\Pi = 1.9 \times 10^{-3}$ μM s^{-1} corresponding to a production of 6.7 μM of PI4P per hour at PI4K/L = 1/100 (Fig. 2*F*), $k_{sac1} = 0.0028$ s^{-1} corresponding to the rate of PI4P hydrolysis by 100 nM Sac1p (15) and $r = 0.015 \pm 0.0009$ μM^{-1} s^{-1}, corresponding to the rate of lipid exchange between Osh4p and a membrane (determined by mixing Osh4p-PI4P complex with liposomes containing different amounts of DHE, *SI Appendix*, Fig. S6). We found that as PI4P production starts in the L_G membrane, p_G increases; hence, Osh4p starts to extract PI4P from L_G membranes and release sterol. Consequently, the increase in PI4P concentration in L_G membranes results in the transport of sterol from L_E to L_G membranes (Fig. 3*B*). To better analyze this result, we considered the following reaction on both kinds of liposomes:

$$op + s \rightleftharpoons os + p. \quad [1]$$

Assuming that Osh4p has the same affinity for sterol and PI4P (11), forward and backward reaction rates are considered equal. Reaction (**1**) is at equilibrium in L_G membranes if $p_o \times s_G = s_o \times p_G$. When p_G starts to build up, the reaction moves backward, and thus, s_G and p_o increase (Fig. 3*B* and *SI Appendix*, Fig. S7), in line with the notion that PI4P accumulation in L_G membranes drives sterol transport to these. In L_E membranes, the opposite occurs: Reaction (**1**) is at equilibrium if $p_o \times s_E = s_o \times p_E$, but Sac1p hydrolyzes PI4P; thus, p_E decreases, reaction (**1**) moves forward, and s_E decreases. Therefore, as long as PI4P is synthesized in L_G membranes, both p_G and s_G increase, and as long as PI4P is hydrolyzed in L_E membranes, both p_E and s_E decrease. The above argument shows that for sterol to be transported from L_E to L_G membranes, $p_o \times s_G < s_o \times p_G$ and $p_o \times s_E > s_o \times p_E$ hence:

$$\frac{s_G}{p_G} < \frac{s_E}{p_E}. \quad [2]$$

Eq. **2** signifies that net sterol transfer occurs from L_E to L_G membranes as long as the sterol-to-PI4P molar ratio is lower in L_G than in L_E membranes. In our simulations, condition (**2**) was confirmed (Fig. 3*C*). Interestingly, a perhaps counterintuitive conclusion is that the maintenance of a low sterol-to-PI4P molar ratio in Golgi-mimetic membranes compared to ER-mimetic membranes is compatible with a transfer process that yields a higher absolute concentration of sterol in Golgi- than in ER-mimetic membranes ($s_G > s_E$).

Next, we show that after longer times, the sterol transfer rate increases and can eventually equal the PI4P synthesis rate (Fig. 3*D*

Downloaded from https://www.pnas.org by 88.122.22.207 on November 5, 2024 from IP address 88.122.22.207.

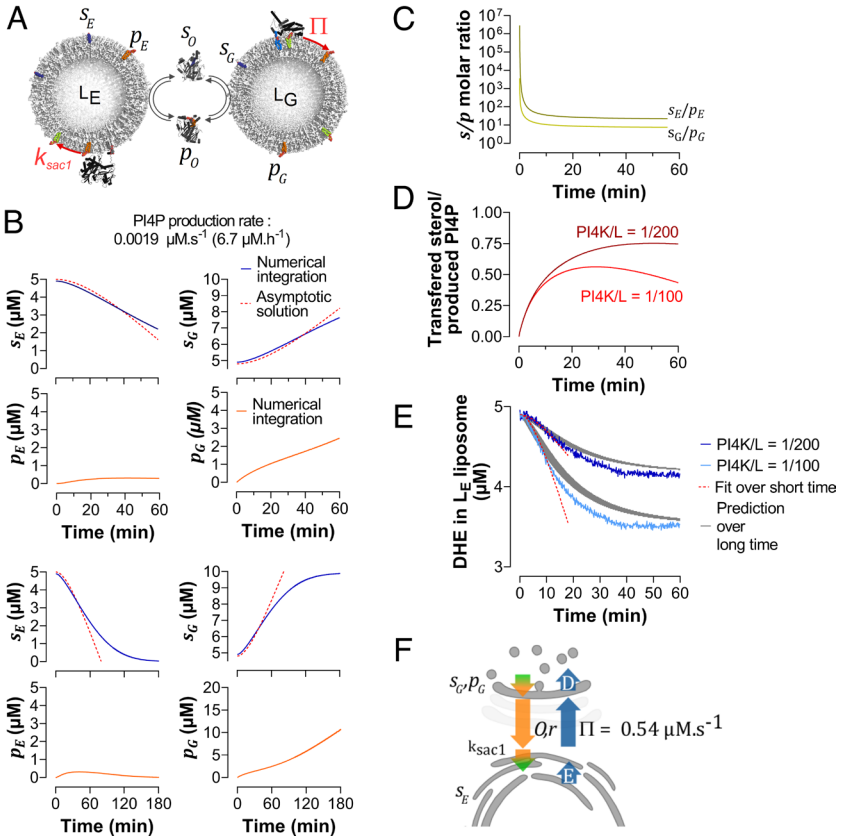

Fig. 3. Kinetic model of ORP-mediated lipid exchange driven by PI4P metabolism. (*A*) Description of the kinetic model. (*B*) Evolution of the sterol and PI4P concentration in the ER-mimetic membrane (s_E, p_E) and Golgi-mimetic membrane (s_G, p_G) for 1 h (*Top*) or 3 h (*Bottom*) according to the model. The initial concentration of sterol s_E and s_G is equal to 5 µM with $O = 200$ nM and $\Pi = 1.9 \times 10^{-3}$ µM s^{-1}, similar to the conditions of DHE transfer assays (Fig. 2*E* with PI4K/L = 1/100). The values were obtained by numerically integrating the full system (*SI Appendix*, Eq. **S9**) (blue or orange) or by an asymptotic analysis of the full system (dashed red line). (*C*) Evolution of the s_E/p_E and s_G/p_G ratio over time in the system. (*D*) Evolution of the ratio of sterol transfer from ER-mimetic to Golgi-mimetic membranes to PI4P production in the Golgi-mimetic membrane with $\Pi = 7 \times 10^{-4}$ or 1.9×10^{-3} µM s^{-1}. (*E*) Analysis of Osh4p-mediated DHE transfer curves shown in Fig. 2*E* (PI4K/L = 1/100 and 1/200) corrected for spontaneous signal decrease. The short-term asymptotic values were fitted to the first 100 data points of the curve considering $O = 200$ nM and $\Pi = 7 \times 10^{-4}$ or 1.9×10^{-3} µM s^{-1}. A numerical integration of the full kinetic model, considering spontaneous sterol transfer between membranes, provided accurate predictions for the data at all times (gray shades: range of predictions for all admissible r and k_{sac1} values obtained with our fitting procedure). (*F*) Description of the fluxes (sterol in blue, PI4P in orange, PI4P hydrolysis and synthesis in orange-green) and parameters used to estimate ORP-mediated ER-to-Golgi sterol transfer rates in cells (Π). The rate obtained for Osh4p is indicated.

and *SI Appendix*, Figs. S7 and S8). The timescale to reach this equilibrium is obtained from an asymptotic solution of the full system, valid at short times (Fig. 3*B* and *SI Appendix*, Fig. S7, dashed red line). It prescribes that when sterol is initially equilibrated between L_E and L_G membranes, sterol decreases in L_E membranes according to:

$$s_E(0) - s_E(t) = \Pi(t - 2\tau * (1 - e^{-t/2\tau})), \qquad [3]$$

where

$$\tau = \frac{k_{sac1} + Or}{rOk_{sac1}}. \qquad [4]$$

When $t \gg \tau$, Eq. **3** reduces to $s_E(0) - s_E(t) \sim \Pi t$, which means that after an initial time, transport becomes one-to-one, i.e., for each molecule of PI4P produced in L_G membranes, one sterol gets transported to this membrane. Most importantly, this equation, along with Eq. **4** illuminates the role of PI4P production and hydrolysis in Osh4p-mediated sterol transfer: If the PI4P production rate (Π) increases, sterol transfer increases (Eq. **3**), and if k_{sac1} increases, τ decreases according to Eq. **4** which results in a faster sterol transfer (Eq. **3**). Moreover, these equations indicate that if the concentration of Osh4p and/or its exchange efficiency r increase, τ decreases (Eq. **4**) which results in a faster sterol transfer (Eq. **3**). Thus, we show that the ability of ORPs to transfer lipids unidirectionally is directly proportional to their concentration, their exchange capacity, and the rate of PI4P synthesis and hydrolysis.

Numerical simulations showed that when $t \gg \tau$, the rate of sterol transfer increased, reaching almost the rate of PI4P synthesis Π (Fig. 3*D*, with parameters chosen as described below). Moreover, over a longer time, these simulations showed that sterol transport slows down and stops once all sterol has been depleted from L_E membranes and has accumulated entirely in L_G membranes (Fig. 3*B* and *SI Appendix*, Fig. S8). Overall, our model correctly predicts that the synthesis of PI4P enables sterol transfer from L_E to L_G membranes, exactly as seen in vitro. However, in our assays, a nontrivial equilibrium was reached before the complete depletion of sterol in the L_E membrane (Fig. 2*E*) which was inconsistent with the model. The likely reason is that spontaneous sterol transfer occurred between L_E and L_G liposomes (*SI Appendix*, Fig. S5*B*), counteracting the directional Osh4p-mediated sterol transfer between these liposomes. Therefore, we included an additional term in the model that accounts for spontaneous sterol transfer (*SI Appendix*, Eq. **S16**).

Downloaded from https://www.pnas.org by 88.122.22.207 on November 5, 2024 from IP address 88.122.22.207.

Finally, we directly compared the full theory (including spontaneous transfer) and the experimental results. The PI4P synthesis rate Π was set to 7.2×10^{-4} μM s^{-1} and 1.9×10^{-3} μM s^{-1} to match our experimental data regarding PI4P production [2.6 and 6.7 μM PI4P in 1 h at PI4K/L = 200 and 100, respectively (Fig. 2*F*)]. k_{sac1} and r were obtained by fitting the first 100 s of the DHE transfer kinetics reported in Fig. 2*E* with the asymptotic solution (Eq. **3**) yielding $k_{sac1} = 0.015 \pm 0.009$ s^{-1} and $r = 0.08 \pm 0.05$ μM^{-1} s^{-1} consistent with the k_{sac1} from ref. 15 and r estimated from our experiments (*SI Appendix*, Fig. S6). We then fitted the long-term equilibrium data to obtain the rate of spontaneous exchange, $C = (4.7 \pm 0.3) \times 10^{-4}$ s^{-1} and $C = (6.6 \pm 0.2) \times 10^{-4}$ s^{-1} at PI4K/L = 1/100 and PI4K/L = 1/200, respectively. Given these parameters, we numerically solved the full model and obtained quantitatively accurate predictions for the data at all times (Fig. 3*E*) for low and high kinase density. This indicates that our model provides a good explanation for the in vitro data.

Prediction on the Coupling between Sterol/PI4P Exchange and PI4P Metabolism in Cells. Next, we used our model to estimate to which extent ORP-mediated lipid exchange coupled to PI4P metabolism can maintain sterol distribution at the ER/Golgi interface in yeast and human cells. We assumed that cell membranes have a relatively stable lipid composition, hence that lipid transport is at equilibrium. Sterol transfer in cells at equilibrium is needed because the established sterol distribution is constantly perturbed as sterol is synthesized in the ER and exported from the *trans*-Golgi by vesicular trafficking. To account for these processes, two terms were added to our model (constant rate E and D, *SI Appendix*, Eq. **S17**). To drive ER-to-Golgi sterol transport and offset the loss of sterol in the Golgi, the rate of sterol and PI4P production, PI4P hydrolysis and lipid exchange must match the rate of sterol export. However, our model predicts that PI4P production can only replenish sterol depletion up to a maximum amount determined by the concentration of Osh4p (OSBP in human cells), O, its lipid exchange rate, r, and the sterol concentration in the ER, s_E (*SI Appendix*):

$$\Pi^* = rOs_E. \quad [5]$$

The actual sterol transport rate, Π, is smaller than Π^* and could be estimated based on additional parameters, i.e., the hydrolysis rate of Sac1p (k_{sac1}) and sterol and PI4P concentration in the Golgi membrane (s_G, p_G) (*SI Appendix*, Eq. **S23**). To obtain these parameters, we carefully collected information on the features of yeast and HeLa cells (internal volume, area of the ER and Golgi membranes, sterol and PI4P content in these membranes, Osh4p and Sac1p copies per yeast, OSBP and SAC1ML copies per HeLa cell) (*SI Appendix*). We estimated that $O = 0.67$ μM, $s_E = 337$ μM, $s_G = 172$ μM in a yeast cell, and plugging these values into *SI Appendix*, Eq. **S23** considering $r = 0.08$ μM^{-1} s^{-1} and $k_{sac1} = 0.06$ s^{-1}, we obtained an ER-to-Golgi sterol transport rate $\Pi = 0.54$ μM s^{-1} (Fig. 3*F* and *SI Appendix*, Table S1). At equilibrium, the PI4P synthesis rate should be equivalent. However, we estimated that the actual rate is likely lower (0.44 μM s^{-1}) considering the level of Pik1p in yeast and its intrinsic activity (43) (*SI Appendix*). Given that Osh4p extracts half the Golgi PI4P pool (34), we estimated that Osh4p might consume PI4P at a rate of 0.24 μM s^{-1}, which is indeed of the same order of magnitude, but slightly lower than the predicted ER-to-Golgi sterol transport rate. We conclude that Golgi PI4P production matches the ballpark needs for sterol transport and may be slightly limiting for Osh4p activity but is potentially sufficient to guarantee the renewal of Golgi sterol pool (s_G) in ~15 min.

For HeLa cells, we estimated that $O = 0.364$ μM and $s_G = 404$ μM. For the concentration of sterol in the ER membrane, we considered two scenarios—either OSBP only has access to a pool of sterol present in ER patches engaged in ER-Golgi contact sites or to sterol contained in the whole ER membrane—and obtained two estimates ($s_E = 67.5$ or 844 μM) and predictions for the rate of ER-to-Golgi sterol transport ($\Pi =$ 0.04 or 0.44 μM s^{-1}). Considering the PI4P level in HeLa cells (44) and considering that inhibition of OSBP leads to a twofold increase in this level in 1 h (17), we estimated that the OSBP/SAC1ML axis could use up to 660 μM PI4P per hour to transfer an equivalent amount of sterol, which is compatible with our first scenario (as 3,600× 0.04 μM s^{-1} = 144 μM sterol transferred per hour). We thus predict that OSBP can partially renew the Golgi sterol pool (400 μM) in 1 h, in line with data showing that this protein ensures 30 to 60% of ER-to-Golgi sterol transfer (17).

Sec14p-Mediated PI Transfer Promotes Osh4p-Mediated Sterol Transfer via PI4P Metabolism. In yeast, Sec14p is a PI/PC exchanger that works with Pik1p to maintain Golgi PI4P levels. Intriguingly, the activities of Sac1p and Osh4p counteract those of Sec14p and Pik1p (32, 34–36). Because the ER is the source of PI, these observations suggest that Sec14p and, more generally, the PI-transfer proteins move PI from this organelle to the *trans*-Golgi and PM to support PI-to-PI4P conversion and possibly ORP-mediated lipid exchange. To test this idea, we examined whether Sec14p could transfer PI from ER- to Golgi-mimetic membranes and promote PI4P synthesis by PI4K. L_E liposomes composed of DOPC/soy PI/Rhod-PE (78/20/2) were incubated with L_G liposomes devoid of PI and coated with PI4K (Fig. 4*A*). Soy PI was selected for these assays because it is more similar to yeast PI species than liver PI (3), and is recognized by Sec14p (45). NBD-PH_{FAPP} was mixed with the liposomes; then Sec14p (200 nM) and ATP were added simultaneously. This elicited a high increase in fluorescence within 1 h, suggesting that NBD-PH_{FAPP} was increasingly bound to L_G membranes in which no Rhod-PE was present to quench the NBD signal. Without Sec14p or ATP, a much lower and no increase were measured, respectively. All these observations suggested that PI was transferred by Sec14p from L_E to L_G liposomes and converted into PI4P by PI4K in the presence of ATP. Confirming this, we observed that adding Osh4p caused a decrease in fluorescence, suggesting that PI4P was present in L_G membranes and transferred by the protein to L_E membranes (Fig. 4*B*). Mirror experiments in which Rhod-PE was incorporated in L_G instead of L_E membranes, provided opposite signals: The fluorescence of NBD-PH_{FAPP} slightly decreased when Sec14p and ATP were added, suggesting that NBD-PH_{FAPP} bound to L_G liposomes due to PI4P synthesis (*SI Appendix*, Fig. S9*A*). The subsequent injection of Osh4p caused an increase in this signal, meaning that the sensor relocated to L_E liposomes following PI4P transfer (*SI Appendix*, Fig. S9*B*). These data suggest that Sec14p can promote PI4P synthesis by delivering PI to membranes onto which PI 4-kinases are present and that Osh4p can counteract Sec14p by removing PI4P from these membranes.

Additionally, we tested an alternative model that could have explained our observations. It assumes that Sec14p presents PI in an optimal configuration to class II and III PI 4-kinases, thereby increasing their enzymatic activity. PI/PC exchange cycles occurring on the membrane onto which kinase is present, with

Downloaded from https://www.pnas.org by 88.122.22.207 on November 5, 2024 from IP address 88.122.22.207.

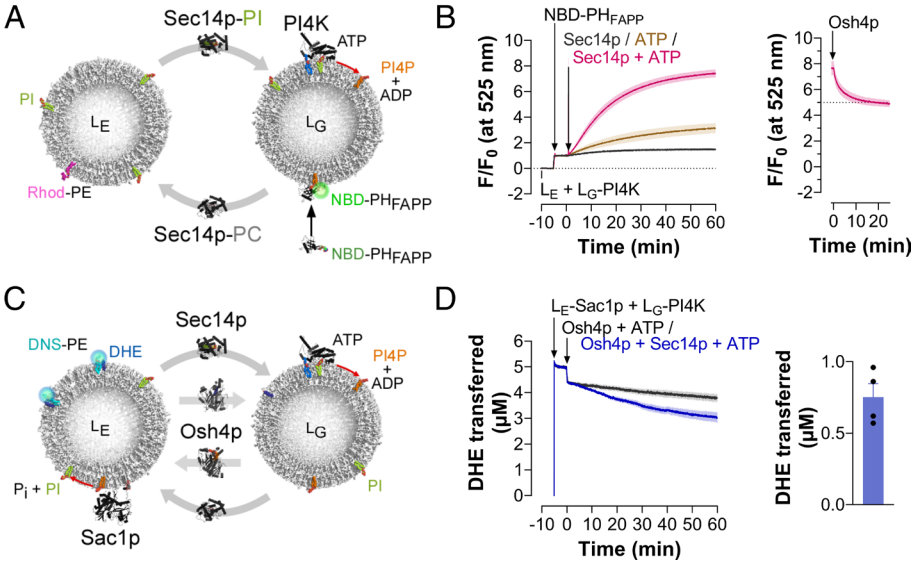

Fig. 4. Sec14p-mediated PI transfer supports PI4P synthesis and Osh4p activity. (*A*) L_G liposomes (200 μM lipids), composed of DOPC/MPB-PE (97/3) and functionalized with PI4K (PI4K/L = 200), were mixed with an equal amount of L_E liposomes composed of DOPC/soy PI/Rhod-PE (78/20/2). NBD-PH_{FAPP} (250 nM) was subsequently added. Five minutes later, ATP and Sec14p (200 nM) were injected alone or in association. Fluorescence was measured at 525 nm (λ_{ex} = 460 nm). The signal was normalized to the F_0 fluorescence measured before the last injection. Mean ± SEM (gray trace, Sec14p only, n = 3; brown trace, ATP only, n = 3; Sec14p and ATP, pink trace, n = 6). (*B*) At the end of kinetics measured in the presence of Sec14p and ATP, shown in (*A*), Osh4p (200 nM) was added, causing a decrease in fluorescence suggestive of a transfer of PI4P from L_G to L_E liposomes. The signal was normalized to the F_0 signal measured in (*A*). Mean ± SEM (n = 3). (*C*) DHE transfer assays. L_E liposomes composed of DOPC/soy PI/DHE/DNS-PE/DOGS-NTA-Ni^{2+} (73/20/2.5/2.5/2), coated with Sac1p[1-522]His_6, were added to L_G liposomes composed of DOPC/MPB-PE/DHE (94.5/3/2.5) and functionalized with PI4K (PI4K/L = 1/200). The concentration of L_E and L_G liposomes was identical. Then, Osh4p (200 nM) and ATP, with or without 200 nM Sec14p, were injected. Mean ± SEM (n = 4). (*D*) Amount of DHE transferred by Osh4p from L_E to L_G liposomes within 1 h in the presence of ATP and Sec14p. Mean ± SEM (n = 4).

no intermembrane lipid transfer, would guarantee this mechanism (33, 37). Using NBD-PH_{FAPP}, we measured the activity of PI4K attached to PI-rich liposomes in the absence or presence of a stoichiometric amount of Sec14p (*SI Appendix*, Fig. S9*C*). In both cases, we recorded similar fluorescence traces suggesting that Sec14p did not boost the synthesis of PI4P. Furthermore, we tested whether Sec14p could activate PI4KIIIβ, a mammal class III PI 4-kinase homologous to Pik1p (26, 31). When 1 μM of purified PI4KIIIβ (*SI Appendix*, Fig. S9*D*) was mixed with PI-rich liposomes and NBD-PH_{FAPP}, we observed a fast increase in signal upon ATP addition (*SI Appendix*, Fig. S9*E*). This was not observed when this experiment was repeated in the presence of 1 μM PIK93, a known inhibitor of PI4KIIIβ, or using liposomes devoid of PI. These data suggested that the signal increase reflected a PI4KIIIβ-dependent PI4P synthesis. Finally, we mixed PI4KIIIβ (250 nM) with PI-rich liposomes in the presence or absence of Sec14p (250 nM) and observed that the latter did not activate the kinase (*SI Appendix*, Fig. S9*F*). These data indicate that Sec14p does not promote the synthesis of PI4P by boosting the catalytic activity of PI 4-kinases.

Finally, we examined whether Sec14p could promote Osh4p-mediated sterol transfer by providing PI to PI4K, thereby supporting PI4P synthesis. To this end, we conducted DHE transfer assays with L_E liposomes containing 20% PI, 2.5% DHE, functionalized with Sac1p, and L_G liposomes containing 2.5% DHE but no PI and covered with PI4K (Fig. 4*C*). Adding Osh4p and ATP did not cause any noticeable DHE transfer from L_E to L_G liposomes, suggesting that no PI4P was generated to support Osh4p activity. In contrast, adding Osh4p, Sec14p, and ATP resulted in sterol transfer (0.75 μM DHE, Fig. 4 *C* and *D*). These data show that a PI-transfer protein can support the lipid transfer activity of an ORP by promoting PI4P synthesis through PI delivery to membranes.

Discussion

How lipid transfer processes are coupled to lipid metabolism has been poorly described quantitatively. In particular, it has been unclear to what extent PI4P metabolism drives ORP-mediated lipid transfer and thereby contributes to creating lipid asymmetries throughout the cell (9). To gain more quantitative insights, we analyzed in vitro how a PI4P gradient generated by a PI 4-kinase and Sac1 between two membranes can drive sterol/PI4P exchange. Moreover, we examined whether a PI-transfer process could assist sterol/PI4P exchange by promoting PI4P synthesis.

Supporting our initial model of sterol/PI4P exchange (11), various studies provided clues that a PI4P gradient at the ER/Golgi, ER/PM, ER/endosome, and ER/lysosome interface is able to pilot vectorial sterol or PS transfer by ORPs (12–14, 16–18, 20, 46). Notably, it has been shown that ORPs transfer activity can be impacted by the inactivation of Sac1 (13, 14). Alternatively, it has been demonstrated that ORPs defective in recognizing PI4P cannot transport a counterligand (12–14, 16, 20). Here, using a controlled system with chemically defined liposomes and recombinant proteins, we fully demonstrate that PI4P synthesis can drive the vectorial transfer of lipids by an ORP and the formation of a lipid gradient between membranes.

First, we report that under initial conditions where sterol is evenly distributed between two membranes, Osh4p can enrich one membrane with sterol, when PI4P is synthesized in this membrane, at the expense of the other. Second, we show that the amplitude of the sterol gradient generated by Osh4p is higher in the presence of Sac1p, which can hydrolyze PI4P and maintain the PI4P gradient generated by PI4P synthesis and dissipated by sterol/PI4P exchange. Finally, we demonstrate that ATP energy is needed not only to create lipid asymmetry across membranes by ATP-dependent flippases and floppases (47) but also lipid gradients between membranes.

Downloaded from https://www.pnas.org by 88.122.22.207 on November 5, 2024 from IP address 88.122.22.207.

Quantitatively, we observed that during the creation of a sterol gradient by Osh4p, the net transfer of one sterol molecule required the synthesis of more than one molecule of PI4P. This seems at odds with our previous study showing that a sterol gradient can be created by the one-for-one exchange of sterol for PI4P (15). However, those results were obtained under conditions where Osh4p could immediately use a preexisting PI4P gradient to generate the sterol gradient. Then, this one was quickly dissipated due to the re-equilibration of sterol between the membranes (15). Here, in a more realistic system where PI4P is continually synthesized and hydrolyzed, PI4P builds up slowly both in membranes and in complexes with Osh4p, which explains why the transfer of one molecule of sterol requires the production of more than one molecule of PI4P. Furthermore, because PI4P synthesis and DHE transfer occur slowly, the spontaneous transfer of sterol between liposomes in a stirring condition is non-negligible and counteracts the creation of a sterol gradient. These two factors explain why there is no one-to-one ratio between the amount of synthesized PI4P and transferred sterol in our system.

Considering these observations and parameters such as PI4P synthesis and hydrolysis rates, the sterol/PI4P exchange rate, and the lipid and protein concentration, we built a kinetic model that provided a good fit for our in vitro data. In particular, this model elucidates how the speed of sterol transport depends on the production of PI4P in Golgi-mimetic membranes and dephosphorylation in ER-mimetic membranes. Importantly, it indicates that sterol can be moved by Osh4p from one membrane to a second one as long as the sterol/PI4P molar ratio is lower in the second membrane than in the first. Presumably, a similar principle drives vectorial PS transfer by PS/PI4P exchange. Therefore, the fact that the total amount of PI4P is much lower than that of sterol or PS in cells is not an obstacle per se for the vectorial transfer of these lipids between organelles. This is precisely what we observed in vitro: Osh4p establishes a vectorial flux of sterol as soon as the synthesis of a few molecules of PI4P starts in the presence of a high amount of sterol. This observation also suggests that a vectorial transfer of sterol and PS by ORPs can be guaranteed as long as the PI4P concentration gradient is steeper than that of sterol and PS at the interface between the ER and other organelles, which is the case considering the intracellular distribution of these three lipids (5–8, 48).

Using our model, we further estimated how much sterol could be transferred from ER to Golgi membranes under the control of PI4P metabolism in yeast and HeLa cells. Estimations were done by combining parameters derived from in vitro data (intrinsic activity of Osh4p and Sac1p) and others inferred from data on the geometry and lipid content of the ER and Golgi apparatus and the cellular abundance of Osh4p or OSBP and Sac1. We conclude that the amount of Golgi PI4P and PI4P turn-over are compatible with maintaining sterol level in the Golgi membrane by Osh4p and OSBP. We also made surprising observations by gathering recent and disseminated data from the literature to feed our model. First, it has been recently reported that in yeast, sterol levels in the ER and Golgi membrane are similar (49). Given the surface area of these two organelles, this means that the sterol pool in the Golgi membrane is lower than that of the ER membrane in terms of intracellular concentration. Second, even if sterol is more concentrated in the Golgi than in the ER membranes of HeLa cells, the sterol pools in the ER and Golgi membranes are predicted to be similar because the ER surface is much greater than that of the Golgi apparatus (50). Moreover, our calculations based on a recent lipidomics study (44) suggest that the PI4P level is comparable to that of sterol in the Golgi apparatus of HeLa cells. All these factors can facilitate robust sterol/PI4P exchange mediated by ORPs at the ER/Golgi interface and explain observations regarding cellular OSBP transfer activity (17).

Our predictions, nevertheless, have limitations. First, our estimation of sterol and PI4P levels in the ER and Golgi membrane likely lacks precision. Notably, it is difficult to estimate the level of sterol in the Golgi apparatus in yeast because, in this cell type, the architecture of this organelle is poorly defined (51), and the number of post-Golgi secretory vesicles is unknown. Second, PI4P also has signaling functions, meaning that our predictions are probably based on an overestimation of the amount of PI4P directly available for exchange with sterol. Third, we cannot precisely determine whether the actual PI4P synthesis rate at the Golgi, which is unknown, matches our predicted rates for ORP-mediated lipid transfer at the ER/Golgi interface. Nevertheless, in the case of HeLa cells, we can rely on reasonable experimental estimates of the amount of PI4P used by OSBP over time (17). However, we must rely on indirect evidence for yeast, i.e., the endogenous expression level of Pik1p and its enzymatic activity measured in vitro (43). Considering that Osh4p uses half of the synthesized Golgi pool (34), an estimation of the PI4P synthesis rate of Pik1p in situ could fully define Osh4p activity. Finally, our model does not consider a factor that can enhance the transfer of sterol to the Golgi by ORPs, which is the high affinity of sterol for saturated phospholipids and/or sphingolipids enriched in this organelle (15).

It is still unclear how Sec14p translates its ability to exchange PC and PI between membranes into a biological function (33, 37). One hypothesis is that Sec14p uses this property to carry PI from the ER to the Golgi to support PI4P production. Alternatively, Sec14p might perform PI/PC exchange only on the Golgi surface to present PI molecules to Pik1p in an optimal configuration for phosphorylation, thereby boosting Pik1p activity (31, 33). Here, our data support the first model: Sec14p can assist the activity of a PI 4-kinase by delivering PI initially contained in another membrane but cannot activate a PI 4-kinase, either of class II or III, already associated with PI-rich membranes. Interestingly, in our assays, Osh4p opposes Sec14p for maintaining a PI4P pool, precisely as observed at the Golgi level (34). More generally, our in vitro data are compatible with the notion that Osh4p can regulate early and later stages of post-Golgi trafficking via its ability to sequester Pik1p-generated PI4P from its effectors in a sterol-dependent manner (22, 33, 52).

Importantly, we observed that Sec14p could promote the sterol/PI4P exchange activity of Osh4p by supporting PI4P synthesis. This strengthens the idea that PI-transfer proteins can support the activity of ORPs, as suggested for PITPβ and OSBP at the interface between the ER and PI4P-rich replication organelles in cells infected by viruses (39). A realistic assumption is that PI-transfer proteins contribute to equilibrating newly made PI at the ER/Golgi interface to maintain PI 4-kinase activity and ORP-mediated lipid exchange.

At the core of our reconstitution assays is a PI 4-kinase that was re-engineered to be covalently attached to liposomes. Intriguingly, PI4K becomes substantially active only in stable association with liposomes. It is likely because it is highly concentrated locally on the membrane surface and can function in a processive mode with continuous access to PI. This might also result from lower mobility of the SSPSC motif, impacting the catalytic site nearby, once it is associated with the membrane (40). However, when PI4K lies on a less fluid membrane, it does not gain efficiency. In contrast, its activity is sensitive to the acyl chain composition of its substrate, as other lipid-synthesizing enzymes and notably PIP 5-kinase (53, 54). We measure the PI4P synthesis rate of a PI 4-kinase bound to a membrane. The activity of PI 4-kinases has previously only

Downloaded from https://www.pnas.org by 88.122.22.207 on November 5, 2024 from IP address 88.122.22.207.

been measured with pure PI or PI/detergent micelles with activation effects caused by detergent (55). However, compared to data obtained in such assays with myristoylated PI4KIIα [150 PI4P/min per protein (56)], we measured a much lower PI4P synthesis rate (0.11 PI4P/min per protein). We do not know which rate more accurately reflects the actual cellular activity of this kinase, but the observed differences are likely due to contrasting experimental designs. In our assays, PI is presented in a bilayer, and PI4K is derived from a truncated version of PI4KIIα (40) that is probably not optimally positioned on the membrane via its link to a phospholipid.

Developing more active versions of the PI4K construct would be interesting. Indeed, the reconstitution of PI4P metabolism between membranes should provide a better understanding of lipid transfer processes and related mechanisms (e.g., contact site formation). More insights might also be gained into how PI-transfer proteins and ORP can function together. It would also help to understand how the ability of PI-transfer proteins to support PI4P synthesis at different membrane interfaces is linked to their capacity to exchange PI for PC or phosphatidic acid [like Nir2 (33, 37)] and to understand the function of enigmatic proteins that comprise a PI-transfer module and an ORD (57).

Experimental Procedures

Protein Purification and Labeling. Osh4p(C98S), Osh4p(C98S/H143A/H144A), NBD-PH_{FAPP}, Sac1p[1-522]His_6, and Sac1p[1-522](C392S)His_6 were purified as previously described (13, 15). The purification of PI4K, Sec14p, and PI4KIIIβ is described in *SI Appendix*. The concentration and folding of proteins were determined by UV spectrometry and circular dichroism, respectively (*SI Appendix*).

Lipids. Phospholipids were purchased from Avanti Polar Lipids, whereas DHE was obtained from Sigma-Aldrich.

Liposome Preparation. Liposomes were prepared in 50 mM HEPES, pH 7.4, and 120 mM K-Acetate (HK) buffer and extruded through polycarbonate filters of 0.2-μm pore size as described in refs. 11 and 15.

Functionalization of Liposomes with PI4K. On the day of the experiment, 100 μL from a stock solution of PI4K was applied onto a Zeba column equilibrated with freshly degassed HK buffer, according to the manufacturer's indications, to remove DTT from the protein. The concentration of the eluted protein was determined by UV spectrometry. Protein at desired concentration was mixed with liposomes (800 μM lipids) composed of DOPC/PI/MPB-PE (87/10/3 mol/mol) for 1 h at 25 °C under agitation. The reaction was stopped by adding 1 mM DTT.

Flotation Assays. Flotation and differential flotation assays were performed as described in ref. 11. See details in *SI Appendix*.

Isolation of Liposomes Coated with PI4K. As described previously, liposomes (800 μM) were functionalized with PI4K (2 μM). Next, a 150-μL volume of the liposome suspension was adjusted to 28% (w/w) sucrose by mixing 100 μL of a 60% (w/w) sucrose solution in HK buffer and overlaid with 200 μL of HK buffer containing 24% (w/w) sucrose and 50 μL of sucrose-free HK buffer. The sample was centrifuged at 240,000 × g in a swing rotor for 1 h. The top fraction (100 μL) in which liposomes are concentrated (~1,200 μM) was used for subsequent experiments.

Fluorescence-Based Kinetics Assays. All kinetics assays were carried out in a Shimadzu RF 5301-PC fluorimeter using a cylindrical quartz cell continuously stirred with a small magnetic bar and thermostated at 30 °C. Liposomes and proteins were injected from stock solutions into the sample through a guide in the cover of the fluorimeter adapted to Hamilton syringes. Protocols to measure PI4K-mediated PI4P synthesis, DHE transport, PI4P transport coupled to PI4P synthesis, PI4P synthesis coupled to PI transport, and PI4P-to-DHE exchange are described in *SI Appendix*.

PI 4-Kinase Assay. PI4K activity was determined by measuring radioactivity from [γ-^{32}P]ATP incorporated into PI using a protocol adapted from ref. 42. See details in *SI Appendix*.

ADP-Glo Assays. Liposomes (200 μM) functionalized or not with PI4K and isolated by a flotation assay were incubated with ultrapure ATP (100 μM, Promega) for 1 h at 30 °C in HK buffer containing 7 mM $MgCl_2$ (HKM7, 100 μL) under shaking. Then, the amount of ADP generated by ATP hydrolysis was determined using the ADP-Glo™ Kinase Assay kit (Promega).

Kinetic Modeling. A full description of the mathematical model used to analyze the in vitro system and provide predictions in cells is given in *SI Appendix*.

Statistical Analyses. Statistical analyses were performed using Prism (GraphPad).

Data, Materials, and Software Availability. Raw data and Matlab source code are available in FigShare with the identifier 10.6084/m9.figshare.25027946. (58). All other data are included in the manuscript and/or supporting information.

ACKNOWLEDGMENTS. We thank Drs. C. Chen, J. Atkinson, and T. Balla for plasmids. This work was supported by a "Défi Modélisation du Vivant-2019" grant from CNRS and "ANR-16-CE13-0006" and "ANR-15-IDEX-0" grants from the Agence Nationale de la Recherche. A.S. acknowledges support from the European Research Council (grant agreement No 101002724 RIDING), the Air Force Office of Scientific Research under award number FA8655-20-1-7028, and the NIH under award number R01DC018789. We thank Y. Van Der Does for manuscript proofreading.

Author affiliations: [a]Université Côte d'Azur, Centre National de la Recherche Scientifique, Institut de Pharmacologie Moléculaire et Cellulaire, Valbonne 06560, France; [b]Department of Physics, École Normale Supérieure (LPENS), Paris 75005, France; and [c]Malga, Department of Civil, Chemical and Environmental Engineering, University of Genoa, Genoa 16145, Italy

1. J. C. Holthuis, A. K. Menon, Lipid landscapes and pipelines in membrane homeostasis. *Nature* **510**, 48–57 (2014).
2. J. Bigay, B. Antonny, Curvature, lipid packing, and electrostatics of membrane organelles: Defining cellular territories in determining specificity. *Dev. Cell* **23**, 886–895 (2012).
3. C. S. Ejsing *et al.*, Global analysis of the yeast lipidome by quantitative shotgun mass spectrometry. *Proc. Natl. Acad. Sci. U.S.A.* **106**, 2136–2141 (2009).
4. J. L. Sampaio *et al.*, Membrane lipidome of an epithelial cell line. *Proc. Natl. Acad. Sci. U.S.A.* **108**, 1903–1907 (2011).
5. B. Mesmin, F. R. Maxfield, Intracellular sterol dynamics. *Biochim. Biophys. Acta* **1791**, 636–645 (2009).
6. I. Levental, K. R. Levental, F. A. Heberle, Lipid rafts: Controversies resolved, mysteries remain. *Trends Cell Biol.* **30**, 341–353 (2020).
7. P. A. Leventis, S. Grinstein, The distribution and function of phosphatidylserine in cellular membranes. *Annu. Rev. Biophys.* **39**, 407–427 (2010).
8. J. G. Kay, G. D. Fairn, Distribution, dynamics and functional roles of phosphatidylserine within the cell. *Cell Commun. Signal.* **17**, 126 (2019).
9. G. Drin, Creating and sensing asymmetric lipid distributions throughout the cell. *Emerg. Top. Life Sci.* **7**, 7–19 (2022).
10. V. Delfosse, W. Bourguet, G. Drin, Structural and functional specialization of OSBP-related proteins. *Contact* **3**, 2515256420946627 (2020).

Downloaded from https://www.pnas.org by 88.122.22.207 on November 5, 2024 from IP address 88.122.22.207.

11. M. de Saint-Jean *et al.*, Osh4p exchanges sterols for phosphatidylinositol 4-phosphate between lipid bilayers. *J. Cell Biol.* **195**, 965–978 (2011).
12. B. Mesmin *et al.*, A four-step cycle driven by PI(4)P hydrolysis directs sterol/PI(4)P exchange by the ER-Golgi tether OSBP. *Cell* **155**, 830–843 (2013).
13. J. Moser von Filseck *et al.*, Phosphatidylserine transport by ORP/Osh proteins is driven by phosphatidylinositol 4-phosphate. *Science* **349**, 432–436 (2015).
14. J. Chung *et al.*, INTRACELLULAR TRANSPORT. PI4P/phosphatidylserine countertransport at ORP5- and ORP8-mediated ER-plasma membrane contacts. *Science* **349**, 428–432 (2015).
15. J. Moser von Filseck, S. Vanni, B. Mesmin, B. Antonny, G. Drin, A phosphatidylinositol-4-phosphate powered exchange mechanism to create a lipid gradient between membranes. *Nat. Commun.* **6**, 6671 (2015).
16. J. Encinar Del Dedo *et al.*, Coupled sterol synthesis and transport machineries at ER-endocytic contact sites. *J. Cell Biol.* **220**, e202010016 (2021).
17. B. Mesmin *et al.*, Sterol transfer, PI4P consumption, and control of membrane lipid order by endogenous OSBP. *EMBO J.* **36**, 3156–3174 (2017).
18. M. Radulovic *et al.*, Cholesterol transfer via endoplasmic reticulum contacts mediates lysosome damage repair. *EMBO J.* **41**, e112677 (2022).
19. J. X. Tan, T. Finkel, A phosphoinositide signalling pathway mediates rapid lysosomal repair. *Nature* **609**, 815–821 (2022).
20. A. Kawasaki *et al.*, PI4P/PS countertransport by ORP10 at ER-endosome membrane contact sites regulates endosome fission. *J. Cell Biol.* **221**, e202103141 (2022).
21. R. Dong *et al.*, Endosome-ER contacts control actin nucleation and retromer function through VAP-dependent regulation of PI4P. *Cell* **166**, 408–423 (2016).
22. C. J. Stefan *et al.*, Membrane dynamics and organelle biogenesis–Lipid pipelines and vesicular carriers. *BMC Biol.* **15**, 102 (2017).
23. R. J. Smindak *et al.*, Lipid-dependent regulation of exocytosis in S. cerevisiae by OSBP homolog (Osh) 4. *J. Cell Sci.* **130**, 3891–3906 (2017).
24. Y. Ling, S. Hayano, P. Novick, Osh4p is needed to reduce the level of phosphatidylinositol-4-phosphate on secretory vesicles as they mature. *Mol. Biol. Cell* **25**, 3389–3400 (2014).
25. M. Sohn *et al.*, PI(4,5)P(2) controls plasma membrane PI4P and PS levels via ORP5/8 recruitment to ER-PM contact sites. *J. Cell Biol.* **217**, 1797–1813 (2018).
26. A. Audhya, M. Foti, S. D. Emr, Distinct roles for the yeast phosphatidylinositol 4-kinases, Stt4p and Pik1p, in secretion, cell growth, and organelle membrane dynamics. *Mol. Biol. Cell* **11**, 2673–2689 (2000).
27. M. Foti, A. Audhya, S. D. Emr, Sac1 lipid phosphatase and Stt4 phosphatidylinositol 4-kinase regulate a pool of phosphatidylinositol 4-phosphate that functions in the control of the actin cytoskeleton and vacuole morphology. *Mol. Biol. Cell* **12**, 2396–2411 (2001).
28. C. J. Stefan *et al.*, Osh proteins regulate phosphoinositide metabolism at ER-plasma membrane contact sites. *Cell* **144**, 389–401 (2011).
29. J. G. Pemberton *et al.*, Defining the subcellular distribution and metabolic channeling of phosphatidylinositol. *J. Cell Biol.* **219**, e201906130 (2020).
30. J. P. Zewe *et al.*, Probing the subcellular distribution of phosphatidylinositol reveals a surprising lack at the plasma membrane. *J. Cell Biol.* **219**, e201906127 (2020).
31. G. Schaaf *et al.*, Functional anatomy of phospholipid binding and regulation of phosphoinositide homeostasis by proteins of the sec14 superfamily. *Mol. Cell* **29**, 191–206 (2008).
32. H. Hama, E. A. Schnieders, J. Thorner, J. Y. Takemoto, D. B. DeWald, Direct involvement of phosphatidylinositol 4-phosphate in secretion in the yeast Saccharomyces cerevisiae. *J. Biol. Chem.* **274**, 34294–34300 (1999).
33. A. Grabon, V. A. Bankaitis, M. I. McDermott, The interface between phosphatidylinositol transfer protein function and phosphoinositide signaling in higher eukaryotes. *J. Lipid Res.* **60**, 242–268 (2019).
34. G. D. Fairn, A. J. Curwin, C. J. Stefan, C. R. McMaster, The oxysterol binding protein Kes1p regulates Golgi apparatus phosphatidylinositol-4-phosphate function. *Proc. Natl. Acad. Sci. U.S.A.* **104**, 15352–15357 (2007).
35. M. P. Rivas *et al.*, Pleiotropic alterations in lipid metabolism in yeast sac1 mutants: Relationship to "bypass Sec14p" and inositol auxotrophy. *Mol. Biol. Cell* **10**, 2235–2250 (1999).
36. S. D. Stock, H. Hama, D. B. DeWald, J. Y. Takemoto, SEC14-dependent secretion in Saccharomyces cerevisiae. Nondependence on sphingolipid synthesis-coupled diacylglycerol production. *J. Biol. Chem.* **274**, 12979–12983 (1999).
37. N. F. Lipp, S. Ikhlef, J. Milanini, G. Drin, Lipid exchangers: Cellular functions and mechanistic links with phosphoinositide metabolism. *Front. Cell Dev. Biol.* **8**, 663 (2020).
38. D. Peretti, N. Dahan, E. Shimoni, K. Hirschberg, S. Lev, Coordinated lipid transfer between the endoplasmic reticulum and the Golgi complex requires the VAP proteins and is essential for Golgi-mediated transport. *Mol. Biol. Cell* **19**, 3871–3884 (2008).
39. P. S. Roulin *et al.*, Rhinovirus uses a phosphatidylinositol 4-phosphate/cholesterol counter-current for the formation of replication compartments at the ER-Golgi interface. *Cell Host Microbe* **16**, 677–690 (2014).
40. Q. Zhou *et al.*, Molecular insights into the membrane-associated phosphatidylinositol 4-kinase IIα. *Nat. Commun.* **5**, 3552 (2014).
41. G. J. Downing, S. Kim, S. Nakanishi, K. J. Catt, T. Balla, Characterization of a soluble adrenal phosphatidylinositol 4-kinase reveals wortmannin sensitivity of type III phosphatidylinositol kinases. *Biochemistry* **35**, 3587–3594 (1996).
42. S. Nakanishi, K. J. Catt, T. Balla, A wortmannin-sensitive phosphatidylinositol 4-kinase that regulates hormone-sensitive pools of inositolphospholipids. *Proc. Natl. Acad. Sci. U.S.A.* **92**, 5317–5321 (1995).
43. C. A. Flanagan, J. Thorner, Purification and characterization of a soluble phosphatidylinositol 4-kinase from the yeast Saccharomyces cerevisiae. *J. Biol. Chem.* **267**, 24117–24125 (1992).
44. P. Li, M. Lämmerhofer, Isomer selective comprehensive lipidomics analysis of phosphoinositides in biological samples by liquid chromatography with data independent acquisition tandem mass spectrometry. *Anal. Chem.* **93**, 9583–9592 (2021).
45. T. Sugiura *et al.*, Biophysical parameters of the Sec14 phospholipid exchange cycle. *Biophys. J.* **116**, 92–103 (2019).
46. Y. Wakana *et al.*, The ER cholesterol sensor SCAP promotes CARTS biogenesis at ER-Golgi membrane contact sites. *J. Cell Biol.* **220**, e202002150 (2021).
47. R. L. López-Marqués *et al.*, Structure and mechanism of ATP-dependent phospholipid transporters. *Biochim. Biophys. Acta* **1850**, 461–475 (2015).
48. G. R. Hammond, G. Schiavo, R. F. Irvine, Immunocytochemical techniques reveal multiple, distinct cellular pools of PtdIns4P and PtdIns(4,5)P(2). *Biochem. J.* **422**, 23–35 (2009).
49. J. Reinhard *et al.*, A new technology for isolating organellar membranes provides fingerprints of lipid bilayer stress. bioRxiv [Preprint] (2022). https://doi.org/10.1101/2022.09.15.508072 (Accessed 16 September 2022).
50. L. Heinrich *et al.*, Whole-cell organelle segmentation in volume electron microscopy. *Nature* **599**, 141–146 (2021).
51. D. Preuss, J. Mulholland, A. Franzusoff, N. Segev, D. Botstein, Characterization of the Saccharomyces Golgi complex through the cell cycle by immunoelectron microscopy. *Mol. Biol. Cell* **3**, 789–803 (1992).
52. C. T. Beh, C. R. McMaster, K. G. Kozminski, A. K. Menon, A detour for yeast oxysterol binding proteins. *J. Biol. Chem.* **287**, 11481–11488 (2012).
53. Y. V. Shulga, R. A. Anderson, M. K. Topham, R. M. Epand, Phosphatidylinositol-4-phosphate 5-kinase isoforms exhibit acyl chain selectivity for both substrate and lipid activator. *J. Biol. Chem.* **287**, 35953–35963 (2012).
54. D. Barneda, S. Cosulich, L. Stephens, P. Hawkins, How is the acyl chain composition of phosphoinositides created and does it matter? *Biochem. Soc. Trans.* **47**, 1291–1305 (2019).
55. T. Balla, Phosphoinositides: Tiny lipids with giant impact on cell regulation. *Physiol. Rev.* **93**, 1019–1137 (2013).
56. B. Barylko *et al.*, Palmitoylation controls the catalytic activity and subcellular distribution of phosphatidylinositol 4-kinase II{alpha}. *J. Biol. Chem.* **284**, 9994–10003 (2009).
57. A. Arabiotorre, V. A. Bankaitis, A. Grabon, Regulation of phosphoinositide metabolism in Apicomplexan parasites. *Front. Cell Dev. Biol.* **11**, 1163574 (2023).
58. G. Drin, Reconstitution of ORP-mediated lipid *exchange* coupled to PI4P *metabolism*. FigShare. https://doi.org/10.6084/m9.figshare.25027946. Deposited 19 January 2024.

Downloaded from https://www.pnas.org by 88.122.22.207 on November 5, 2024 from IP address 88.122.22.207.